Mechanical stretch induced collective cell alignment

Xuechen Shi[1,2,#] and Sulin Zhang[1,3,4,#]

[1]Department of Biomedical Engineering, Pennsylvania State University, University Park, Pennsylvania 16802, United States

[2]Department of Physiology, University of Pennsylvania, Philadelphia, Pennsylvania 19104, United States

[3]Department of Engineering Science and Mechanics, Pennsylvania State University, University Park, Pennsylvania 16802, United States

[4]Department of Material Science and Engineering, Pennsylvania State University, University Park, Pennsylvania 16802, United States

Corresponding author: xuechen.shi@pennmedicine.upenn.edu, suz10@psu.edu

Abstract

Cell alignment is a fundamental process in development and plays an essential role in tissue function. Although it has been found that cell alignment exhibits a density-dependent collective behavior, the collective mechanisms within this process remain elusive. In this study, we present a model of collective cell alignment induced by uniaxial mechanical stretch and explore the mechanisms driving this phenomenon. We demonstrate that alignment occurs in a density-dependent manner, with dense cell populations aligning while sparse populations do not. Contrary to previous findings, our results show that this alignment is initiated by substrate deformation upon stretch, which biases cell orientations towards the stretched direction. This deformation-induced alignment occurs passively and simultaneously, allowing us to isolate and identify the factors contributing to the collective behavior. Importantly, we find that once stretched, cells in low-density cultures lose alignment over time, while cells in high-density cultures are able to maintain the alignment level, exhibiting positional adaptation. Furthermore, we observe a self-organization process in high-density cultures, where cells actively reorient towards the stretched direction through cell-cell interactions, enhancing the overall alignment level over time. The emergence of the alignment response has implications for how cell alignment is achieved and sheds light on the cooperative mechanisms underlying collective cell behaviors. Additionally, our findings introduce a novel methodology for aligning cells that could be used for biomedical and tissue engineering applications.

Introduction

Cell alignment, a process where cellular polarization is directed in a designated direction, is crucial for forming highly regulated and patterned tissue morphologies. It exists in various tissue types and plays an indispensable role in coordinating multiple physiological functions with tissue architectures. For example, myoblasts align during myogenesis and muscle regeneration, which is essential for the fusion of individual cells into multinucleated myotubes and the formation of skeletal muscle(*1, 2*). In blood vessels, endothelial cells align in the direction of the laminar shear stress created by blood flow, and the impairment of this alignment is associated with inflammation reactions, endothelial apoptosis, and atherosclerosis(*3, 4*). Fibroblasts align along the parallel collagen fibrils in tendons and ligaments, which is essential for producing collagen matrices during the injury healing process(*5-7*). Due to the ubiquity and importance of cell alignment, numerous methodologies have been developed to replicate this behavior in vitro for both fundamental research and engineering applications(*8-12*) , and various molecular and mechanical factors involved in mechanotransduction pathways responsible for alignment have been identified(*2, 13-19*). Nevertheless, several key aspects of the mechanisms that enable this multicellular, highly regulated, and organized architecture remain incompletely understood.

Recent findings have shown that cell-cell interactions provide collective mechanisms directing behaviors that are unachievable by individual cells. For instance, cells in dense colonies exhibit faster and more correlated responses to ATP stimulation compared to sparsely distributed cells, a phenomenon termed collective chemosensing(*20, 21*). Studies combining experiments and simulations have provided fundamental insights into how cells collectively sense shallow chemical gradients through cell-cell communication(*22-24*). In collective chemotaxis, cells migrate collectively following concentration gradients, whereas individual cells do not(*25, 26*). Beyond chemical signals, cells exhibit collective responses to mechanical cues. In collective durotaxis, multicellular clusters recognize and migrate towards stiffer regions of a substrate, a response not observed in isolated cells(*27*). Our lab has demonstrated a metastasis model in human colon carcinoma (HCT-8) colonies, where cells in smaller colonies were more prone to malignant progression and cell dispersion(*28*). Moreover, it has been found that on a cylinder with macroscale curvature, confluent fibroblasts align along the cylinder's axial direction, while sparsely cultured cells show much weaker alignment(*29*). On weak topographic patterns, C2C12 myoblasts achieve global alignment in confluent culture, whereas individual cells do not align on such patterned substrates(*30*). Although these studies used different triggers to induce various collective cell responses, a common finding is that increased cell density enhances the degree of these behaviors. In contrast, cells at lower density exhibit such behaviors only when exposed to greater magnitudes of the triggers. This feature indicate that the interaction between cells allows them to exchange information and increase sensitivity to environmental cues. However, in the context of cell alignment, the specific mechanisms by which cell-cell interactions facilitate collective alignment responses remain to be explored. Central to this challenge is the difficulty in separating triggers that result in individual cell alignment from the cooperative machinery where cell-cell interaction occurs, as the former typically involves complex mechanotransduction pathways and biomechanical responses.

In this paper, we create a simple methodology to establish an alignment model to explore the collective mechanisms driving cell alignment. Cell alignment was initially induced by uniaxial mechanical stretch, which could be applied with different magnitudes to control the alignment level. Notably, we observed that alignment occurred in a density-dependent manner, indicating the existence of a collective feature. Further experiments and analyses demonstrated that individual cell alignment was solely induced by geometric apposition that was transferred from the substrate generated by the stretch. This approach allowed us to focus on the collective aspects of alignment without overlapping with the signaling pathways that initiate alignment. We observed that, once stretched, cells in closely packed clusters exhibited reinforcement in alignment, whereas cells at lower densities gradually lost alignment. We further revealed that the self-enhancement of alignment was mediated by cell-cell interactions that facilitated the exchange of positional information. Together, our findings provide insights into cooperative mechanisms that may universally direct organized cell behaviors and introduce a new methodology for aligning cells for biomedical applications.

Results

1. Mechanical stretch induces collective alignment

We first observe the collective behavior in cell alignment under static uniaxial mechanical stretches using C2C12 myoblasts. Poly(dimethylsiloxane) (PDMS) elastic membranes are coated with fibronectin to promote cell adhesion and are loaded onto stretch devices. C2C12 cells are seeded on the membranes and are able to attach to the membrane substrates, spreading within four hours of seeding. When allowed to proliferate to confluence, the cells exhibit random orientations without alignment (Fig. 1A and Fig. S1A). To apply uniaxial stretch, cells are seeded on the stretch device at varying densities and incubated overnight. Subsequently, static uniaxial stretches are applied three times with a magnitude of 15% each time (45% in total), with a four-hour interval between each stretch loading. Stretch loading is applied using a distance controller, which regulates the stretch magnitude and takes only a few seconds for the stretching action. We note that the stretch does not alter cell viability, as confirmed by cell viability assay (Fig. S2). We image the cells and determine the levels of cell alignment under different conditions at the next day after the stretch. Remarkably, when the cell density is near-confluence at 725 cells/mm² before the stretch, significant cell alignment is observed (Fig. 1B and Fig. S1B). However, when the cells are at a sub-confluent, low density of 68 cells/mm², the stretch is unable to induce alignment (Fig. 1C), even as the cells proliferate to a much higher density at later stages (Fig. S1C and Fig. S1D). The levels of cell alignment, represented as alignment index (see Methods), are presented under these conditions (Fig. 1D).

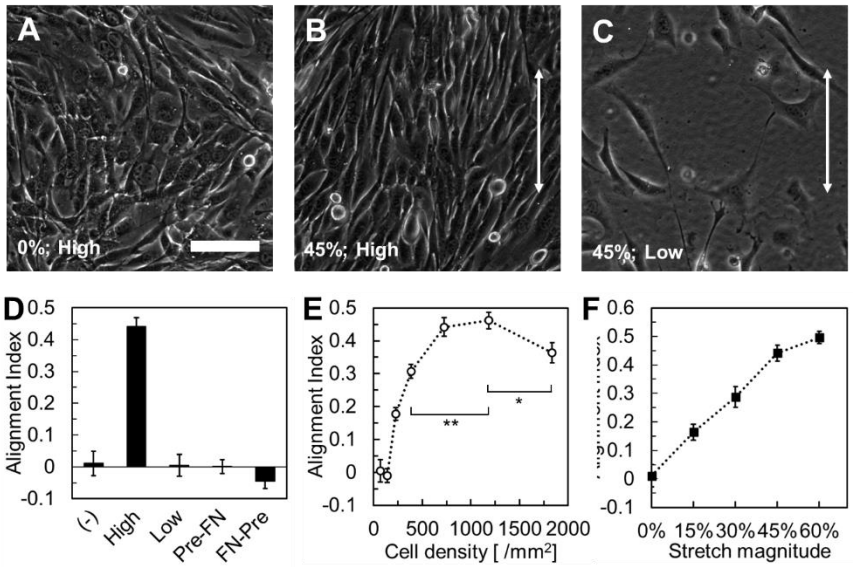

Figure 1. Mechanical stretch induced collective alignment. **A**. Random cell orientations at high cell density without static mechanical stretch. **B**. Cell alignment with 45% mechanical stretch at high cell density. **C**. Random cell orientations with 45% mechanical stretch at low cell density. **D**. Average alignment indexes under different conditions. (-) indicates no stretch at high cell density. High: high cell density with 45% stretch. $p<0.001$ between "High" and all other groups. Low: low cell density with 45% stretch. Pre-FN: pre-stretch of the substrate before fibronectin coating prior to cell seeding at high density. FN-Pre: pre-stretch of the substrate after fibronectin coating prior to cell seeding at high density. **E**. Effect of cell seeding density on cell alignment with 45% mechanical stretch. *$p<0.05$; **$p<0.01$. **F**. Effect of stretch magnitude on cell alignment with a high cell density. In each condition, static stretches are applied three times evenly with a cell density of 730 cells/mm². $n\geq3$ for each condition. For each alignment index, analyzed cell number>1000. Scale bar: 100 μm.

We next investigate cell alignment at different cell densities. In all conditions, three stretch loadings are applied as described above, with a total stretch magnitude of 45%. The results show that cell alignment increases with cell density until it reaches a plateau, beyond which the alignment decreases slightly with further increases in cell density (Fig. 1E). We also study the effects of stretch magnitudes on cell alignment. In each group, cells in high density are stretched three times with the total stretch magnitude distributed evenly among each stretch, with a four-hour interval between each loading. Across different groups with the same cell density before the stretch, but varying stretch magnitudes, the final alignment is measured at hour 30. We observe that cell alignment is strongly regulated by the stretch magnitudes (Fig. 1F). Together, here we demonstrate a collective mode of cell alignment induced by static mechanical stretches, where dense cells align while isolated cells do not.

2. Cell alignment is initiated by substrate deformation

We then investigated the mechanism behind cell alignment. First, we find that cells at high density cannot align on a pre-stretched substrate with the same stretch magnitude, regardless of whether fibronectin is coated before or after the stretch (Fig. 1D). Therefore, changes in substrate material properties, such as ECM fiber alignment(*31, 32*), topography changes(*33, 34*), or stiffness anisotropy(*16*), are not responsible for the observed

alignment. In addition, it is unlikely that alignment is achieved through soluble factors in the culture medium, as the diffusion of soluble molecules is isotropic and cannot lead to the formation of a polarized, anisotropic alignment pattern in large scale.

Studies have reported that mechanical tension applied to the substrate can immediately regulate the direction of cell migration(*35, 36*) and increase cell traction force(*37*). Building on this, we hypothesize a kinetic mode where C2C12 cells respond to mechanical stretch and alter their orientation angles towards the stretching direction, leading to cell alignment. To assess the contribution of this mechanism, we first examine the change in cell traction force with mechanical stretch. Unlike published results with NIH/3T3 fibroblasts(*37*), we do not observe an increased traction force in C2C12 myoblasts on 21 kPa polyacrylamide hydrogel (Fig. S3), indicating that these cells may not actively respond to mechanical stretch. To further test the active re-orientation process, we manually measure the change in cell angle in both low and high culture densities after a stretch with a magnitude of 15%. The angle change represents the difference in cell orientational angle immediately after stretch application and that after 2 or 4 hours. A positive angle change indicates re-orientation towards the stretch direction, while a negative angle change indicates re-orientation away from it. In both low and high densities, we find no inclination for cells to realign towards the stretched direction after 15% stretch (Fig. S4), while cells in confluent culture density exhibit a lesser deviation from the stretched direction. Therefore, we do not attribute the collective alignment of cells to their ability to sense and actively respond to mechanical forces.

We note that during stretch loading, cells deform along with the substrate, a phenomenon that can be visualized and quantified using fluorescent beads beneath the cells (Fig. 2A-B). This deformation biases cell orientation, causing it to shift towards the direction of stretch, potentially inducing cell alignment. To investigate the contribution of this mechanism, we first examine the relationship between the deformation of the substrate due to stretch and the resulting cell deformation. The “deformation ratio” is defined as the ratio of resulting cellular deformation to substrate deformation in the stretched direction (y), where “deformation” is determined by the ratio of the projected post-stretch length to the pre-stretch length in the y direction. We observe that when cells in high density are stretched by 15%, the deformation ratio is near 1 regardless of the initial cell orientation (Fig. 2C), indicating that cells almost have the same deformation along with the substrate. Additionally, due to the Poisson effect, the stretch in the y direction is accompanied by compression in the x direction. Thus, we quantify the cell deformation along with the substrate in the x direction, and the results show that cells are also deformed in the x direction with the same deformation ratio (Fig. 2C). To assess the impact of the nearly 100% deformation ratio, we proceed to analyze how substrate deformation leads to cell deformation and rearrangement. This process can be effectively modeled by scaling and resizing the image according to the substrate deformation due to the stretch (Fig. S5A and B). Interestingly, the computationally scaled image closely resembles the bright field image of the stretched cells (Fig. S5C), which revealed a consistent global yet passive alignment of the cells. We next observe that cellular deformation transferred from the substrate directly influences cell alignment, as evidenced by comparing the alignment levels of cells before and immediately after stretching (Fig. 2D-E).

Collectively, these findings suggest that cells adhere almost fully to the substrate, deforming together with the substrate during stretch, which provides a mechanism for the observed cell alignment.

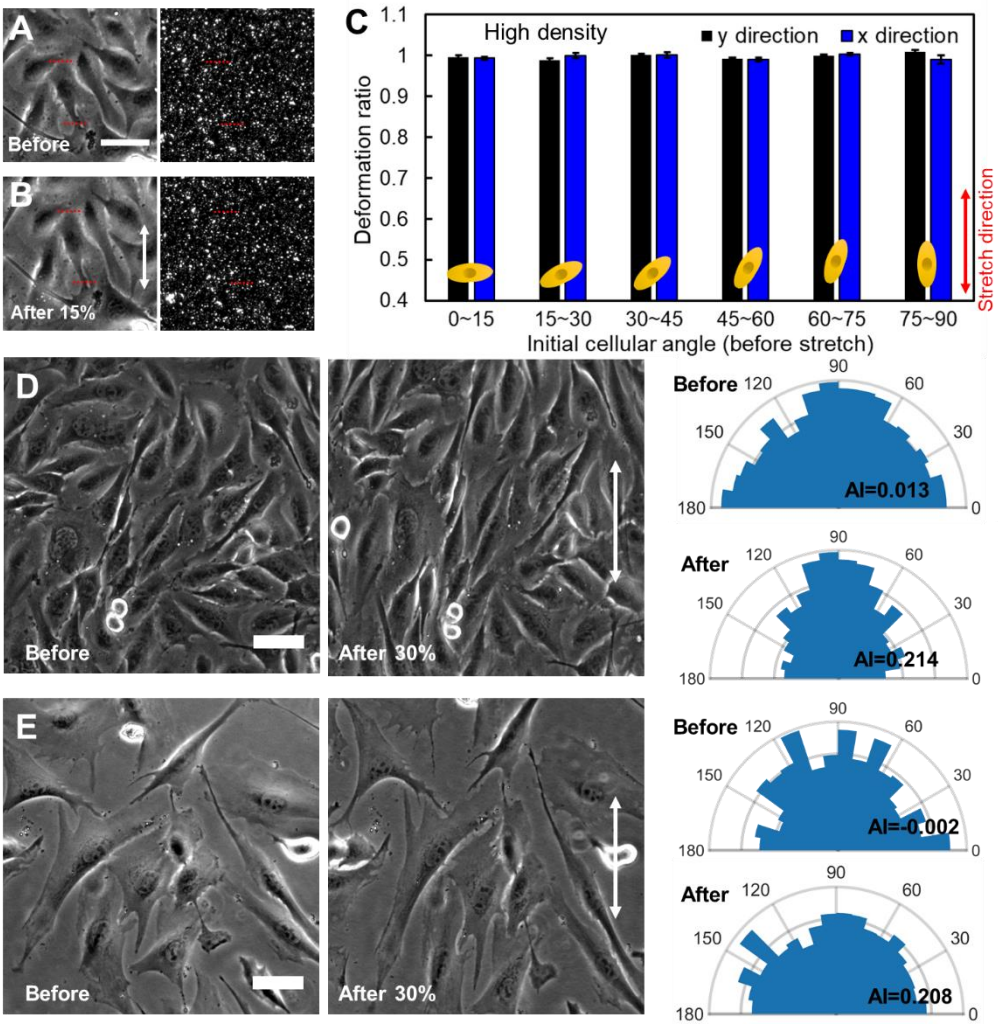

Figure 2. Deformation-initiated cell orientation bias and the resulting cell alignment. **A** and **B**. The position of a cell relative to the fluorescent beads-coated substrate before (A) and after (B) 15% uniaxial stretch. Red lines denote the top and bottom boundaries of the cell in the bright field image, corresponding to the locations in the fluorescent channel. **C**. Deformation ratio (defined in the Methods section) of cells in high density (590/mm^2) after 15% mechanical stretch in terms of initial cell orientational angles in the y (stretched direction, red arrow) or x directions. n≥5 for each column. p>0.3 for each group compared with "1". **D** and **E**. Immediate cell alignment as a result of 30% mechanical stretch in high (D, 620/mm^2) and low (E, 130/mm^2) cell densities. The right panels present rose-plots for the cell angle distributions before and after the stretch, with indicated alignment index. n>1000 for each rose-plot. Scale bar: 50 μm.

3. Collective alignment involves positional adaption and self-organization

While the deformation-induced alignment mechanism is a straightforward process, it fails to explain why cells in low density do not exhibit alignment the following day and thereafter. First, substrate deformation is transferred to cells in both low and high culture densities, both exhibiting a deformation ratio near 1 (Fig. S6A). Secondly, it is worth noting that the cell angle change generated by stretch-induced deformation, and hence the

alignment level, is a function of the cell aspect ratio (Fig. S6B): the larger the aspect ratio, the less tendency there is to bias the cell orientation. We thus investigate whether cell aspect ratio depends on cell culture density, and we find no significant difference in aspect ratios between low and high densities (Fig. S6C). Since deformation ratio and aspect ratio are the sole factors determining cell angle bias given a same stretch magnitude, these results explain that immediately after a stretch, the alignment levels for cells in both low and high densities be the same, as illustrated above (Fig. 2D-E, and Fig. S6D). Therefore, the difference in final alignment levels, despite the same immediate alignment levels after the stretch, must arise from collective mechanisms following the stretch. We thus predict that after substrate deformation initiates cell alignment, cooperative mechanisms synergistically regulate the final alignment levels.

We next study how cooperative mechanisms are involved in substrate deformation-induced cell angle rearrangement and hence the collective cell alignment. Notably, upon a stretch of 35% magnitude, cells in low culture density gradually lose substrate deformation-induced angle change and alignment over time (Fig. 3A and Fig. S7A). In contrast, cells in higher culture density increase their alignment level (Fig. 3A and Fig. S7B). Given sufficient substrate deformation, the decreasing alignment in low cell density explains why cell alignment occurs in high cell density but not in low cell density, as cells in lower density eventually lose their alignment, thus providing a mechanism for collective alignment. Similar observations have been reported previously, where isolated cells reorient freely while in cell clusters cellular movements are trapped, believed to be associated with contact inhibition of locomotion mediated by cell density(*38-41*). We term this feature *positional adaptation*, as cells in higher densities better adapt to their orientational position, while those in lower densities do not. Positional adaptation in confluent cells may be attributable to relatively frozen cell movement in confluent densities, mediated by cell density and the strengthening of cell adhesions(*42, 43*).

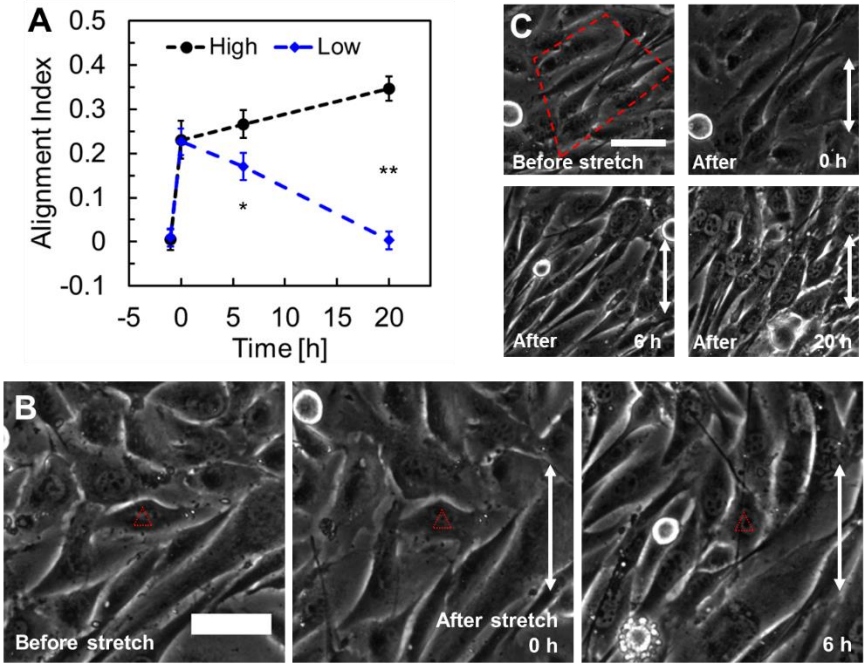

Figure 3. Collective features contributing to cell alignment. **A**. Cell alignment levels over time for high (570/mm^2) and low (160/mm^2) culture densities after a 35% static stretch. *p=0.068; **p<10^{-6}. n≥5. **B**. Cell angle change influenced by neighboring cells after a 30% stretch in high culture density (800/mm^2). The representative cell, indicated by the red triangle, was initially oriented in the x direction thus could not passively reorient via substrate deformation. After 6 hours, this cell aligned in the stretched y direction (white arrow), a phenomenon that was accompanied by neighboring aligned cells. For n=12 cells that are x-direction oriented surrounded by partially aligned cells that we analyzed, all eventually showed y-direction alignment. **C**. Representative image showing the inability to align for cells in an unaligned oriented domain in high culture density (800/mm^2). Among n=25 such oriented domains analyzed, none showed alignment, and all became nematic defects eventually. Scale bar: 50 μm.

In addition to positional adaption, cells in high density actively re-arrange their angles towards the stretched direction, gradually increasing the alignment level (Fig. 3A), indicating a self-organization process that enhances alignment. To dissect the determinants of this response, we first observe the reorientation process of cells initially polarized perpendicular (x) to the stretch direction (y). These cells tend not to align via the deformation transferred from the substrate, as the deformation only changes their aspect ratios, not their orientations. Importantly, cells initially polarized near the x direction can still reorient to the y direction upon stretch if accompanied by neighboring aligned cells (Fig. 3B), supporting the existence of active reorientation and self-organization. Conversely, self-organization is ineffective in cells surrounded by unaligned cells. Some C2C12 cells, upon reaching confluence, spontaneously form oriented domains or parallel arrays(*39, 40*), where adjacent cells align in the same direction (Fig. S8). These oriented domains can be somewhat aligned by stretch-generated substrate deformation but are resistant to further alignment through self-organization, eventually forming nematic defects (Fig. 3C). These results indicate that self-organization-based alignment requires the presence of adjacent aligned cells; re-orientation is unlikely to occur if none of the surrounding cells is aligned, as seen inside unaligned oriented domains.

Together, we herein identify two collective mechanisms that drive cell alignment after the initial, low-level alignment induced by stretch: positional adaptation, which is the ability of cells in higher densities to better adapt to their orientational positions compared to cells in lower densities, and self-organization, where cells in high-density cultures actively rearrange their angles towards the stretched direction, gradually increasing the overall alignment level.

4. Cell-cell interaction during the self-organization process

To provide direct evidence of the self-organization process during cell alignment, we hypothesize that unaligned cells, through cell-cell interaction, can align with adjacent aligned cells, leading to self-organization and overall alignment increase. To test this hypothesis, we separate the self-organization process from the stretch-induced initial alignment process via a "secondary seeding experiment" (Fig. 4A). First, we seed cells at a near-confluent density (230/mm^2) and stretch them three times, with a total stretch magnitude of 45% (Fig. 4B). This density is chosen so that the losing of alignment (Fig. 3A and Fig. S7A) is small. Immediately after the stretch, we seed a second group of cells with the same density into the same culture, achieving a high overall culture density. We observe that the second groups of cells attach to the substrate and spread within 1.5 hours, without overlapping

on the initially seeded cells (Fig. 4C). After overnight incubation, we observe that the alignment level of all the cells reaches the same level as that of cells seeded at a near-confluent density without the second group (Fig. 4D, Fig. S9A-B). Although we cannot isolate and quantify the alignment level of only the secondary cells, the overall alignment level suggests that the secondary cells align by following the orientation of the initially seeded cells. Conversely, if the two groups of cells are seeded simultaneously before the stretch (i.e., seeding only once at double density), the alignment level would be twice that of the secondary seeding experiment (Fig. 4D, Fig. S9C). We propose that the secondly seeded cells do not undergo the initial alignment process through the stretch but instead align by following the initially seeded cells, which limits the overall alignment level. Together, these results confirm the existence of cell-cell interaction that enables cells to re-orient with their surrounding cells, resulting in self-organization behavior that contributes to the collective alignment.

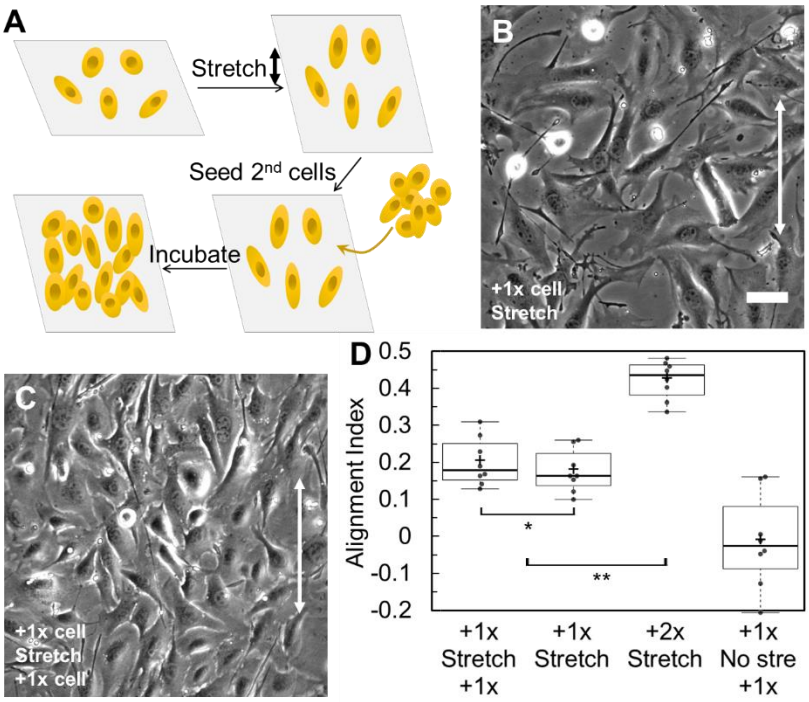

Figure 4. Self-organization process during cell alignment. **A**. Schematic of the "secondary seeding experiment" to distinguish the self-organization process from the initial alignment induced by uniaxial stretch. **B**. Bright field image of cells after 45% stretch. "+1x cell" indicates that cells are initially seeded at a near-confluent 1x density (230/mm^2); "Stretch" indicates that the cells are subsequently subjected to a 45% stretch. **C**. Bright field image of the culture 1.5 hours after seeding the secondary cells. "+1x cell" below "Stretch" indicates that after stretching, an additional 1x density of cells is seeded into the culture. **D**. Quantification of cell alignment levels with or without secondary seeding after overnight incubation. First column: the "secondary seeding experiment" as described in C. Second column: no second group of cells is seeded after the stretch. Third column: initially 2x density of cells is seeded, and the stretch is applied, but no second group of cells is seeded. Last column: same as the "secondary seeding experiment" except that no stretch is applied. *$p>0.1$; **$p<10^{-5}$. $n\geq5$. Scale bar: 50 μm.

To further investigate how self-organization enhances initial cell alignment, we explore how cells interact to exchange positional information. Studies suggest that cells are able to communicate mechanically through elastic

media(*16, 44-46*). However, we believe that the collective mechanisms here do not involve cell-cell interaction through the underlying PDMS substrate. Dividing the maximal cell traction force (~1 kPa) by the shear modulus of PDMS (~1 MPa) yields a substrate strain of approximately 0.1%, far below the minimal threshold (~2.5%) required to be sensed by adjacent cells(*45*). To further test whether cells communicate through traction forces on the soft substrate, we apply laser ablation to determine how cellular force is influenced by an interruption in cell-cell interaction. We seed cells on a 2.6 kPa soft polyacrylamide hydrogel and incubate them with gold nanorods before the laser ablation experiments. To combine traction force microscopy (TFM) with laser ablation, we identify a pair of closely situated cells and capture an image of fluorescent beads underneath them (image I). Next, we open the laser shutter and apply a laser beam to ablate one of the cells for about 20 seconds. After laser ablation, we close the laser shutter and record the fluorescent beads underneath the cells (image II). Finally, we use a drop of sodium hydroxide solution to detach the cells and record the final image of the fluorescent beads (image III). By comparing images I and III, we obtain the traction force of the cell pair; by comparing images II and III, we obtain the traction force of the individual cell. Comparing the traction force before and after laser ablation (Fig. S10), we do not observe a significant contribution from the ablated cell, indicating that cell-cell mechanical interaction through the soft substrate minimally affects another cell. Future experiments should investigate other mechanisms of cell-cell interactions that give rise to the self-organization, such as through gap junctions or physical cell-cell contact.

Summary

In this study, we demonstrate a collective mode of cell alignment, where cells in high-density cultures align under uniaxial mechanical stretch, while cells in low-density cultures do not. The alignment process is initiated by uniaxial mechanical stretch, which induces substrate deformation, subsequently causing geometric cell reorientation. As mechanical stretch generates similar initial alignment in cells regardless of culture density, this alignment approach allows us to identify the factors responsible for the collective nature of the alignment process. We identify two main mechanisms driving the collective behaviors: positional adaption and self-organization. Positional adaption occurs when cells in high-density cultures maintain their orientation potentially due to restricted movement and strong cell adhesions. Self-organization involves unaligned cells aligning with adjacent aligned cells through cell-cell interactions, leading to a continues increase in cell alignment level with time. Our findings not only enhance our understanding of the cooperative mechanisms that may universally exist and direct organized cell behaviors and tissue morphologies, but also provide a simple methodology to align cells for skeletal muscle tissue engineering applications.

Materials and Methods

Cell culture and treatment

Mouse skeletal myoblasts (C2C12) were cultured in Dulbecco's Modified Eagle Medium (DMEM, Millipore-Sigma) supplemented with 10% (v/v) fetal bovine serum (FBS, R&D Systems) and 1% (v/v) penicillin-streptomycin (R&D Systems). Cells at passage numbers 10-13 were used in the experiments. All cells were incubated at 37°C in an incubator with 5% CO_2 and 90% humidity. To quantify cell angles, cell nuclei were stained with Hoechst 33342 (Thermo Fisher) at 0.5 μg/ml for 10 minutes.

In vitro stretch application

A stretching device was adapted to uniaxially stretch the cells. The cell stretcher (Electron Microscopy Sciences) comprised a rectangular PDMS membrane that could be mechanically stretched, a membrane chamber for holding the membrane, and a digital distance controller to control the stretch magnitude. This setup allowed for different magnitudes of uniaxial stretch within the membrane. To enable cell attachment, PDMS substrates were incubated with fibronectin (Millipore-Sigma) at 0.05 mg/ml for 30 minutes at 37°C. Upon stretching the cells on the PDMS membrane, mechanical stretch was transmitted to adherent cells through cell-substrate interactions. For angle analysis, the stretch direction was defined to be in the y direction (θ=90°).

Quantification of cell alignment

Cell orientation angles were determined using the outline-etching method(*47, 48*), which quantified the angles of cell nuclei to represent cell angles. The degree of cell alignment and directionality to the stretched direction was quantified using an alignment index, a parameter widely used to quantify the alignment level of cells, stress fibers, and ECM fibers(*7, 49-51*). The alignment index (AI) was calculated based on individual cell angle (θ_i):

$$\mathrm{AI} = \frac{1}{\mathrm{N}}\sum_{\mathrm{i}=1}^{\mathrm{N}}[2\cos^2(\theta_\mathrm{i} - 90) - 1]$$

where N is the total number of cells analyzed (in our study for each group N≥150). If all cells are randomized in their angles, $\mathrm{AI} = 0$; if all cells are aligned to the stretched direction ($\theta = 90°$), $\mathrm{AI} = 1$; if all cells are aligned perpendicular to the stretched direction, $\mathrm{AI} = -1$.

Quantification of deformation ratio

During stretch loading, both the PDMS substrate and the cells were deformed. The deformation, in the y (stretching) or x direction, was defined as the relative change in length of the substrate or cells. The deformation ratio, in the y or x direction, was defined as the ratio between the deformation of a cell and the deformation of the substrate region underneath the cell. A deformation ratio of 1 indicates that a cell adheres to the substrate tightly during stretch; a deformation ratio of 0 indicates that a cell does not change its geometry during stretch. To quantify the deformation of the substrate(*52*), the PDMS membranes were labelled with fluorescent beads. Specifically, the membranes were treated with (3-Aminopropyl)triethoxysilane (Millipore-Sigma) at 5% (v/v in

isopropyl alcohol) for 10 minutes and 0.3% carboxylated fluorescent beads (0.2 μm in diameter, Thermo Fisher) for 10 minutes. The substrates were then passivated with 100 mM Tris base (Millipore-Sigma) for 10 minutes prior to fibronectin coating.

Traction force microscopy

To evaluate changes in cell traction forces caused by mechanical stretch, we attached soft polyacrylamide hydrogel to the PDMS membrane as a cell culture substrate based on a previous protocol with modifications(*53*). PDMS membranes were treated with (3-Aminopropyl)triethoxysilane at 10% (v/v in isopropyl alcohol) for 30 minutes, washed thoroughly with isopropyl alcohol and water, and dried. They were then incubated with 1% (v/v in water) glutaraldehyde (Millipore-Sigma) for 2 hours, washed, and dried. The membranes were then ready to be coated with polyacrylamide hydrogels.

Polyacrylamide hydrogels embedded with fluorescent beads (0.2 μm in diameter) were prepared on the functionalized PDMS membranes or coverslips to perform traction force microscopy based on previously published methods(*28, 53*). After polymerization, hydrogels were functionalized with fibronectin (Millipore-Sigma) by the crosslinker Sulfo-SANPAH (Pierce Chemical)(*54, 55*). Traction force was determined by tracing the cell-generated displacement field in the hydrogel by comparing an image pair containing two fluorescent bead configurations in the absence/presence of the cell. To exclude the stretch-generated displacement in the hydrogel from the cell contraction-generated displacement field, the fluorescent image pair was captured with the same stretch magnitude. Initially, an image of the fluorescent beads beneath the cells was taken before applying stretch (image I). The substrate was then stretched, and cells were incubated for 40 minutes, after which a second image of the fluorescent beads was recorded (image II). Sodium hydroxide solution was then added to detach the cells, and a third image of the beads under stretch was captured (image III). Finally, the stretch was released, and a fourth fluorescent image was taken (image IV). Comparing images I and IV provided the traction force of the cells without stretch, while comparing images II and III provided the traction force after stretch loading.

Laser ablation

Laser ablation was used to kill one cell from a cell pair to study cell-cell interaction and communication. Prior to the experiments, cells were incubated with $2x10^{11}$/ml gold nanorods overnight. Laser ablation was conducted by irradiating the cell with a laser tweezer module with a single-mode diode laser (150 mW, 1064 nm) in an epi-fluorescence microscope (Nikon, TE2000-U). Detailed experimental procedures for the laser ablation experiments combined with TFM are presented in the Results section.

Statistical analysis

Statistical analysis was performed using Student's two-tailed t-test. Data are presented as mean ± standard error of the mean (SEM). The significance level of each statistical test is presented with each experimental data.

References

1. M. Wakelam, The fusion of myoblasts. *Biochemical Journal* **228**, 1 (1985).
2. M. Junkin, S. L. Leung, S. Whitman, C. C. Gregorio, P. K. Wong, Cellular self-organization by autocatalytic alignment feedback. *Journal of cell science* **124**, 4213-4220 (2011).
3. A.-C. Vion *et al.*, Autophagy is required for endothelial cell alignment and atheroprotection under physiological blood flow. *Proceedings of the National Academy of Sciences* **114**, E8675-E8684 (2017).
4. D. E. Conway, M. A. Schwartz, Flow-dependent cellular mechanotransduction in atherosclerosis. *Journal of cell science* **126**, 5101-5109 (2013).
5. J. H. Wang, F. Jia, T. W. Gilbert, S. L. Woo, Cell orientation determines the alignment of cell-produced collagenous matrix. *Journal of biomechanics* **36**, 97-102 (2003).
6. Z. Yin *et al.*, The regulation of tendon stem cell differentiation by the alignment of nanofibers. *Biomaterials* **31**, 2163-2175 (2010).
7. K. Chen *et al.*, Role of boundary conditions in determining cell alignment in response to stretch. *Proceedings of the National Academy of Sciences* **115**, 986-991 (2018).
8. S. Kalinina *et al.*, Isothiocyanate-functionalized RGD peptides for tailoring cell-adhesive surface patterns. *Biomaterials* **29**, 3004-3013 (2008).
9. C. Williams *et al.*, Aligned cell sheets grown on thermo‐responsive substrates with microcontact printed protein patterns. *Adv Mater* **21**, 2161-2164 (2009).
10. J. S. Choi, S. J. Lee, G. J. Christ, A. Atala, J. J. Yoo, The influence of electrospun aligned poly (epsilon-caprolactone)/collagen nanofiber meshes on the formation of self-aligned skeletal muscle myotubes. *Biomaterials* **29**, 2899-2906 (2008).
11. J. I. Andersen, C. P. Pennisi, T. Fink, V. Zachar, Focal adhesion kinase activation is necessary for stretch-induced alignment and enhanced differentiation of myogenic precursor cells. *Tissue Engineering Part A* **24**, 631-640 (2018).
12. K. Kurpinski, J. Chu, C. Hashi, S. Li, Anisotropic mechanosensing by mesenchymal stem cells. *Proceedings of the National Academy of Sciences* **103**, 16095-16100 (2006).
13. A. Livne, E. Bouchbinder, B. Geiger, Cell reorientation under cyclic stretching. *Biophysical journal* **106**, 42a (2014).
14. R. Kaunas, P. Nguyen, S. Usami, S. Chien, Cooperative effects of Rho and mechanical stretch on stress fiber organization. *Proceedings of the National Academy of Sciences* **102**, 15895-15900 (2005).
15. Y. Li *et al.*, Engineering cell alignment in vitro. *Biotechnology advances* **32**, 347-365 (2014).
16. I. B. Bischofs, U. S. Schwarz, Cell organization in soft media due to active mechanosensing. *Proceedings of the National Academy of Sciences* **100**, 9274-9279 (2003).
17. R. De, A. Zemel, S. A. Safran, Dynamics of cell orientation. *Nature Physics* **3**, 655-659 (2007).
18. A. Ray *et al.*, Anisotropic forces from spatially constrained focal adhesions mediate contact guidance directed cell migration. *Nature communications* **8**, 14923 (2017).

19. J. H.-C. Wang, P. Goldschmidt-Clermont, J. Wille, F. C.-P. Yin, Specificity of endothelial cell reorientation in response to cyclic mechanical stretching. *Journal of biomechanics* **34**, 1563-1572 (2001).

20. B. Sun, J. Lembong, H. Stone, Spatial-temporal dynamics of collective chemosensing. *Biophysical Journal* **102**, 104a (2012).

21. J. C. Conrad, Quantifying collective behavior in mammalian cells. *Proceedings of the National Academy of Sciences* **109**, 7591-7592 (2012).

22. D. Ellison *et al.*, Cell–cell communication enhances the capacity of cell ensembles to sense shallow gradients during morphogenesis. *Proceedings of the National Academy of Sciences* **113**, E679-E688 (2016).

23. S. Fancher, A. Mugler, Fundamental limits to collective concentration sensing in cell populations. *Physical review letters* **118**, 078101 (2017).

24. A. Mugler, A. Levchenko, I. Nemenman, Limits to the precision of gradient sensing with spatial communication and temporal integration. *Proceedings of the National Academy of Sciences* **113**, E689-E695 (2016).

25. G. Malet-Engra *et al.*, Collective cell motility promotes chemotactic prowess and resistance to chemorepulsion. *Current Biology* **25**, 242-250 (2015).

26. E. Theveneau *et al.*, Collective chemotaxis requires contact-dependent cell polarity. *Dev Cell* **19**, 39-53 (2010).

27. R. Sunyer *et al.*, Collective cell durotaxis emerges from long-range intercellular force transmission. *Science* **353**, 1157-1161 (2016).

28. Y. Zhang *et al.*, A traction force threshold signifies metastatic phenotypic change in multicellular epithelia. *Soft Matter* **15**, 7203-7210 (2019).

29. N. D. Bade, R. D. Kamien, R. K. Assoian, K. J. Stebe, Curvature and Rho activation differentially control the alignment of cells and stress fibers. *Science advances* **3**, e1700150 (2017).

30. M. S. Grigola, C. L. Dyck, D. S. Babacan, D. N. Joaquin, K. J. Hsia, Myoblast alignment on 2D wavy patterns: Dependence on feature characteristics and cell - cell interaction. *Biotechnology and bioengineering* **111**, 1617-1626 (2014).

31. H. H. Vandenburgh, P. Karlisch, Longitudinal growth of skeletal myotubes in vitro in a new horizontal mechanical cell stimulator. *In vitro cellular & developmental biology* **25**, 607-616 (1989).

32. H. H. Vandenburgh, Dynamic mechanical orientation of skeletal myofibers in vitro. *Developmental Biology* **93**, 438-443 (1982).

33. D. J. Evans, S. Britland, P. M. Wigmore, Differential response of fetal and neonatal myoblasts to topographical guidance cues in vitro. *Development genes and evolution* **209**, 438-442 (1999).

34. P. Y. Wang, H. T. Yu, W. B. Tsai, Modulation of alignment and differentiation of skeletal myoblasts by submicron ridges/grooves surface structure. *Biotechnology and bioengineering* **106**, 285-294 (2010).

35. C.-M. Lo, H.-B. Wang, M. Dembo, Y.-l. Wang, Cell movement is guided by the rigidity of

the substrate. *Biophysical journal* **79**, 144-152 (2000).

36. H.-B. Wang, M. Dembo, S. K. Hanks, Y.-l. Wang, Focal adhesion kinase is involved in mechanosensing during fibroblast migration. *Proceedings of the National Academy of Sciences* **98**, 11295-11300 (2001).
37. S. Munevar, Y.-l. Wang, M. Dembo, Regulation of mechanical interactions between fibroblasts and the substratum by stretch-activated Ca2+ entry. *Journal of cell science* **117**, 85-92 (2004).
38. M. Abercrombie, J. E. Heaysman, Observations on the social behaviour of cells in tissue culture: I. Speed of movement of chick heart fibroblasts in relation to their mutual contacts. *Experimental cell research* **5**, 111-131 (1953).
39. L. Edelstein-Keshet, G. B. Ermentrout, Models for contact-mediated pattern formation: cells that form parallel arrays. *Journal of mathematical biology* **29**, 33-58 (1990).
40. L. Petitjean *et al.*, Velocity fields in a collectively migrating epithelium. *Biophysical journal* **98**, 1790-1800 (2010).
41. L. Edelstein-Keshet, G. B. Ermentrout, Contact response of cells can mediate morphogenetic pattern formation. *Differentiation* **45**, 147-159 (1990).
42. G. Duclos, S. Garcia, H. Yevick, P. Silberzan, Perfect nematic order in confined monolayers of spindle-shaped cells. *Soft matter* **10**, 2346-2353 (2014).
43. S. Garcia *et al.*, Physics of active jamming during collective cellular motion in a monolayer. *Proceedings of the National Academy of Sciences* **112**, 15314-15319 (2015).
44. J. P. Winer, S. Oake, P. A. Janmey, Non-linear elasticity of extracellular matrices enables contractile cells to communicate local position and orientation. *PloS one* **4**, e6382 (2009).
45. X. Tang, P. Bajaj, R. Bashir, T. A. Saif, How far cardiac cells can see each other mechanically. *Soft Matter* **7**, 6151-6158 (2011).
46. C. A. Reinhart-King, M. Dembo, D. A. Hammer, Cell-cell mechanical communication through compliant substrates. *Biophysical journal* **95**, 6044-6051 (2008).
47. N. Zhu, H. K. Kwong, Y. Bao, T.-H. Chen, Chiral orientation of skeletal muscle cells requires rigid substrate. *Micromachines* **8**, 181 (2017).
48. Y. Huang, Y. Bao, H. K. Kwong, T. H. Chen, M. L. Lam, Outline - etching image segmentation reveals enhanced cell chirality through intercellular alignment. *Biotechnology and Bioengineering* **115**, 2595-2603 (2018).
49. Y. Pang, X. Wang, D. Lee, H. P. Greisler, Dynamic quantitative visualization of single cell alignment and migration and matrix remodeling in 3-D collagen hydrogels under mechanical force. *Biomaterials* **32**, 3776-3783 (2011).
50. F. Xu, T. Beyazoglu, E. Hefner, U. A. Gurkan, U. Demirci, Automated and adaptable quantification of cellular alignment from microscopic images for tissue engineering applications. *Tissue Engineering Part C: Methods* **17**, 641-649 (2011).
51. M. Sun, A. B. Bloom, M. H. Zaman, Rapid quantification of 3D collagen fiber alignment and fiber intersection correlations with high sensitivity. *PLoS One* **10**, e0131814 (2015).
52. S. R. K. Vedula *et al.*, Mechanics of epithelial closure over non-adherent environments. *Nature communications* **6**, 6111 (2015).

53. L. Casares *et al.*, Hydraulic fracture during epithelial stretching. *Nat Mater* **14**, 343-351 (2015).

54. Q. Wei *et al.*, Actin-ring segment switching drives nonadhesive gap closure. *Proc Natl Acad Sci U S A* **117**, 33263-33271 (2020).

55. X. C. Shi *et al.*, Elastocapillarity at Cell-Matrix Contacts. *Phys Rev X* **12**, (2022).